Computational and Structural Biotechnology Journal 21 (2023) 3159–3172

Contents lists available at ScienceDirect

Computational and Structural Biotechnology Journal

journal homepage: www.elsevier.com/locate/csbj

Research article

Rational design, synthesis and structural characterization of peptides and peptidomimetics to target Hsp90/Cdc37 interaction for treating hepatocellular carcinoma

Surya Sukumaran [a,1], Mingdian Tan [b,1], Shulamit Fluss Ben-Uliel [a], Hui Zhang [b], Marta De Zotti [c], Mei-Sze Chua [b], Samuel K. So [b], Nir Qvit [a,*]

[a] The Azrieli Faculty of Medicine in the Galilee, Bar-Ilan University, Henrietta Szold St. 8, Safed 1311502, Israel
[b] Asian Liver Center, Department of Surgery, Stanford University School of Medicine, 1201 Welch Road, Palo Alto, CA 94305, USA
[c] Department of Chemistry, University of Padova, Via Marzolo 1, 35131 Padova, Italy

ARTICLE INFO

Article history:
Received 1 February 2023
Received in revised form 23 May 2023
Accepted 23 May 2023
Available online 25 May 2023

Keywords:
Hsp90 (heat shock protein 90)
Cdc37 (cell division cycle 37)
HCC (hepatocellular carcinoma)
Peptides
Peptidomimetics
Cyclic peptidomimetics
Pre-cyclic peptidomimetics
Backbone cyclization
Protein-protein interaction
Peptide probes
Field effect biosensing (FEB)
Colocalization
CD (Circular dichroism)

ABSTRACT

Heat shock protein 90 (Hsp90) and cell division cycle 37 (Cdc37) work together as a molecular chaperone complex to regulate the activity of a multitude of client protein kinases. These kinases belong to a wide array of intracellular signaling networks that mediate multiple cellular processes including proliferation. As a result, Hsp90 and Cdc37 represent innovative therapeutic targets in various cancers (such as leukemia, multiple myeloma, and hepatocellular carcinoma (HCC)) in which their expression levels are elevated. Conventional small molecule Hsp90 inhibitors act by blocking the conserved adenosine triphosphate (ATP) binding site. However, by targeting less conserved sites in a more specific manner, peptides and peptidomimetics (modified peptides) hold potential as more efficacious and less toxic alternatives to the conventional small molecule inhibitors. Using a rational approach, we herein developed bioactive peptides targeting Hsp90/Cdc37 interaction. A six amino acid linear peptide derived from Cdc37, KTGDEK, was designed to target Hsp90. We used *in silico* computational docking to first define its mode of interaction, and binding orientation, and then conjugated the peptide with a cell penetrating peptide, TAT, and a fluorescent dye to confirm its ability to colocalize with Hsp90 in HCC cells. Based on the parent linear sequence, we developed a peptidomimetics library of pre-cyclic and cyclic derivatives. These peptidomimetics were evaluated for their binding affinity to Hsp90, and bioactivity in HCC cell lines. Among them, a pre-cyclic peptidomimetic demonstrates high binding affinity and bioactivity in HCC cells, causing reduced cell proliferation that is associated with induction of cell apoptosis, and down-regulation of phosphorylated MEK1/2. Overall, this generalized approach of rational design, structural optimization, and cellular validation of 'drug-like' peptidomimetics against Hsp90/Cdc37 offers a feasible and promising way to design novel therapeutic agents for malignancies and other diseases that are dependent on this molecular chaperone complex.

1. Introduction

Hepatocellular carcinoma (HCC) is the predominant form of adult liver malignancies, accounting for about 75–85% of primary liver cancers. It is the second most lethal malignancy following lung cancer [1,2]. Most HCC patients remain asymptomatic in the early stages of the disease and are diagnosed only in the advanced stages of the malignancy [3,4]. Late diagnosis, together with limited treatment options at the advanced stages and high recurrence rates, underlies the increase in mortality rates of HCC patients globally [5]. HCC patients typically have poor survival outcomes, largely due to the pathophysiologic complexity of HCC which makes it a challenging malignancy to treat. Each of the current treatment strategies (such as radiofrequency ablation, surgical ablation, systemic/combination therapy, and transplantation) has its own limitations, including undesirable side effects and drug resistance [6,7]. A

* Corresponding author.
E-mail address: nir.qvit@biu.ac.il (N. Qvit).
[1] Equal contribution.

https://doi.org/10.1016/j.csbj.2023.05.023

promising approach is to target crucial protein-protein interactions (PPIs) involved in key signalling pathways, such as the PI3K (phosphoinositide 3-kinase)-AKT (protein kinase B)-mTOR (mammalian target of rapamycin), Wnt, EGFR (epidermal growth factor receptor), as well as the heat shock protein 90 (Hsp90) and the cell division cycle 37 (Cdc37) pathways to therapeutically regulate the molecular heterogeneity of HCC [8].

The molecular chaperone-kinome pathway mediated by Hsp90 and Cdc37 is an attractive therapeutic target in various tumors including HCC [9,10]. Hsp90 is among one of the most critically conserved molecular chaperones in eukaryotic cells; it facilitates cell cycle control, protein folding/assembly, signal transduction pathways, and quality control and regulation of proteins [11,12]. Cdc37 is a kinase-specific co-chaperone of Hsp90 which directs and recruits selective client proteins into Hsp90 in an adenosine triphosphate (ATP)-dependent manner, thereby regulating the chaperone kinase signal transduction pathways [13]. Hsp90 cooperates with Cdc37 by regulating the stabilization, folding, and phosphorylation of signal transduction mediators [14]. Hsp90 and Cdc37 have been considered potential anti-tumor targets due to their elevated expression in various malignancies such as acute myeloblastic leukemia, prostate cancer, multiple myeloma, and HCC [10,15].

Currently available Hsp90 inhibitors such as purine and radicicol-based inhibitors, resorcinol, geldanamycin, and benzamide analogues block the N-terminal ATP-binding pocket on Hsp90, thereby leading to client protein degradation *via* inhibiting the chaperone cycle [10,15,16]. The ATPase-mediated inhibition of Hsp90 function affects the degradation of not only oncogenic proteins, but of proteins involved in the normal physiological functioning of the body; this lack of specificity results in diverse side effects which hampered their progress through clinical trials [10,16,17]. Furthermore, the inhibition of ATPase function of Hsp90 commonly leads to the release of heat shock transcription factor-1 (Hsf-1), followed by the activation of compensatory mechanisms that induce the expression of other chaperones, including Hsp70 and Hsp27, resulting in poor Hsp90 inhibitory efficacy [10]. An alternative and more promising approach would be to target Hsp90/Cdc37 PPI using highly selective and therefore less toxic bioactive peptides and peptidomimetics (modified peptides) derived from specific PPI interfaces, rather than inhibiting the non-specific ATPase domain of Hsp90.

Peptides are naturally occurring bioactive chemical tools that can mimic a protein surface, and that possess high selectivity, good efficacy, and low toxicity [18,19]. However, linear peptides suffer from limitations such as poor plasma stability and low oral bioavailability [20]. By introducing chemical modifications to the native linear peptide, these limitations can be overcome. For example, peptidomimetics offer superior metabolic stability, enhanced receptor affinity, increased selectivity, and improved bioavailability [19,21]. Linear peptides offer high conformational flexibility that is important for their interactions with their protein partners. The conformational space of the linear peptide can be explored by the generation of small peptidomimetic libraries [21], which can often lead to the identification of a peptidomimetic with improved binding affinity, stability, bioactivity, and selectivity compared to the linear peptide. Peptidomimetic compounds can be developed mainly through either local (*e.g.*, the incorporation of non-natural amino acids), or global (*e.g.*, cyclization) approaches [22,23].

Large macromolecules including peptides have poor intrinsic cell permeability. This can be overcome by conjugating them to cell penetrating peptides (CPPs), which are short peptides that can facilitate cellular uptake of various cargos [24]. CPPs have shown great potential in delivering otherwise undeliverable therapeutic molecules into cells. Moreover, clinical data from over 25 completed Phase I and Phase II clinical trials have confirmed the safety of using CPPs [25,26]. One of the most commonly used CPP is derived from the trans-activator of transcription (TAT) of the human immunodeficiency viruses (HIV-1) protein (sequence YGRKKRRQRRR) [27].

In this study, we developed a rationally designed linear hexapeptide targeting Hsp90/Cdc37 PPI. To ensure cell internalization, the hexapeptide was conjugated with TAT. We predicted the binding mode of the hexapeptide using *in silico* molecular docking, and validate it by colocalization experiments. We then generated a peptidomimetics library based on the linear hexapeptide, consisting of pre-cyclic and cyclic derivatives; their 3D-structures were then determined using circular dichroism (CD) analysis. We evaluated the binding capabilities, bioactivity, and specificity of the hexapeptide and its peptidomimetics to its target protein, Hsp90. One pre-cyclic peptidomimetic, CHP-028, demonstrated enhanced binding efficacy and cytotoxic activity against HCC cell lines, when compared to the other peptidomimetics and the linear hexapeptide. We successfully demonstrated that the specific and rational approach of peptide design and step-by-step monitoring can be used to effectively advance the development of chemically modified peptidomimetics as more potent 'drug-like' compounds to target the Hsp90/Cdc37 interface in pathological conditions such as HCC.

2. Materials and methods

2.1. Sequence alignment

Sequences from different species were aligned using the Lalign server. The proteins and species used are: Hsp90A proteins from *Homo sapiens* (P07900), *Mus musculus* (P07901), and *Rattus norvegicus* (P082995); Hsp90B proteins from *Homo sapiens* (P08238), *Mus musculus* (P11499), and *Rattus norvegicus* (P34058); and Cdc37 proteins from *Homo sapiens* (Q16543), *Mus musculus* (Q61081), *Rattus norvegicus* (Q63692), and *Gallus gallus* (O57476).

2.2. Molecular docking of peptide with Hsp90

The computational docking studies were performed using the HPEPDOCK2.0 online web server, which performs blind protein-peptide docking through a hierarchical algorithm that enables rapid conformational modelling of peptides. It is particularly well known for its flexible peptide orientation sampling and refinement of different peptide conformations using the MODPEP program [28,29]. The Alpha Fold predicted model of Hsp90, AF-P07900-F1, was used for docking in the HPEPDOCK2.0 server [30]. Initially, the secondary structure of the designed parent linear peptide was generated using Chou & Fasman Secondary Structure Prediction (CFSSP) web server; the PyMol (Schrodinger LLC) software was then used to build the peptide structure based on these coordinates, and to analyze the docked peptide conformations with Hsp90 [31].

2.3. Peptide synthesis

All commercially available solvents and reagents were used without further purification. Dichloromethane (DCM), Piperidine, Diethyl ether, N,N Diisopropylethylamine (DIEA), Trifluoroacetic acid (TFA), and HPLC grade water were purchased from (Bio-Lab, Jerusalem, Israel); HPLC grade acetonitrile (ACN) was purchased from J.T. Baker (Phillipsburg, NJ, USA); Acetic anhydride was purchased from Daejung (Busan, Korea); Triisopropylsilane (TIS) and Succinic anhydride were purchased from Acros (Princeton, NJ, USA); Dimethylformamide (DMF) was purchased from Carlo Erba (Val-de-Reuil, France); Oxyma pure was contributed by Luxembourg Bio Technologies Ltd. (Ness Ziona, Israel); N,N-Diisopropylcarbodiimide (DIC) was purchased from Angene International Limited (Jiangsu,

China); Glutaric anhydride was purchased from Alfa Aesar (Haverhill, MA, USA); Benzotriazole-1-yl-oxy-tris-pyrrolidinophosphonium hexafluorophosphate (PyBOP) was purchased from GL Biochem Ltd (Minhang, China); Fmoc Rink amide AM resin was purchased from Matrix innovation (substitution 0.5 mmol/g, Quebec city, Quebec, Canada); Fmoc-protected amino acids were purchased from Ontores Bioscience (Beijing, China). Side chains of the amino acids used in the synthesis were protected as follows: tert-Butyloxycarbonyl (BOC) (Lys), tert-butyl (tBu) (Thr/Tyr/Glu), t-butyl ester (OtBu) (Asp), 2,2,4,6,7-Pentamethyldihydrobenzofuran-5-sulfonyl (Pbf) (Arg), 4-methyltrityl (Mtt) (Lys), and triphenylmethy (Trt) (Gln).

Parent linear peptide and peptidomimetics were chemically synthesized using a fully automated parallel peptide synthesizer (Syro I, Biotage, Uppsala, Sweden) on solid support by following the solid-phase peptide synthesis (SPPS) methodology [32] with a fluorenylmethoxycarbonyl (Fmoc)/tert-Butyl (tBu) protocol. The linear peptide synthesis starts with Fmoc deprotection and was performed in two steps: 3 min and 12 min, both at 75 °C using piperidine (40%) in DMF solution. Coupling reactions were performed by repetition of the following cycle conditions: 45 min, 75 °C, with DIC (0.2 M) in DMF, Oxyma pure (0.2 M) in DMF, and amino acid (0.2 M) in DMF. After the linear peptide was synthesized, an anhydride spacer was coupled to its N-terminal amino group, and cyclization was performed using amide bonds between the moiety linker at the backbone N-terminus and an epsilon amino on the side chain of a lysine residue [33], which is protected with N-methyltrityl (Mtt, a protection group that can be deprotected selectively using acid labile conditions) [34]. Anhydride coupling was carried out by repetition of the following cycle conditions: 30 min at room temperature, using anhydride (10 eq)/ DIEA (10 eq)/ peptide (1 eq) in DMF. Prior cyclization, Mtt deprotection was carried out using TFA/TIS/DCM (1:5:94 v/v/v), 3 × 5 min at room temperature. Cyclization was performed manually in chemical hood using DCM, and PyBOP/DIEA (5:10), for 3 × 1 h at room temperature. The final cleavage and side chain deprotection was done manually. Peptide cleavage from the resin and deprotection of the amino acid side chains were carried out with a pre-cooled mixture of TFA/TIS/H_2O solution (90:2.5:2.5 v/v/v) for three hours at room temperature. The resin was removed by filtration, and the solvents were evaporated by a stream of compressed air. The crude products were precipitated with diethyl ether, collected by centrifugation, dissolved in CH_3CN /H_2O (30:70), and lyophilized.

Peptides were analyzed by analytical reversed-phase high-pressure liquid chromatography (RP-HPLC) using the 1260 Infinity II LC System (Agilent, Santa Clara, CA, USA) that is equipped with G7129A 1260 vial sampler, G7111B 1260 quaternary pump, G7115A 1260 DAD (Diode Array Detector) WR, G1364C 1260 FC-AS, G1330B 1290 thermostat, from Agilent (Santa Clara, CA, USA) using a Luna 5 μm C18(2) 100 Å (250 × 4.6 mm) column (Phenomenex, Torrance, CA, USA) at 1 mL/min. The solvent systems used were A (H_2O with 0.1% TFA) and B (CH_3CN with 0.1% TFA). A linear gradient of 5–95% B in 45 min was applied and the detection was at 214 nm and 254 nm. Molecular weight characterization was done by matrix assisted laser desorption/ionization mass spectrometry (MALDI-MS) (autoflex® maX, Bruker, Billerica, MA, USA). Peptides were dissolved in a 70:30 solution of (i) 0.1% TFA in HPLC grade water, and (ii) 30% of acetonitrile. The peptide samples were spotted on a stainless-steel MALDI-TOF MTP 384 target plate (Bruker Daltonik GmbH, Bremen, Germany) by mixing 1:1 ratio of 2,5-Dihydroxy benzoic acid (2,5-DHB) matrix and peptide samples.

The synthesized products were purified by preparative RP-HPLC (1260 Infinity II LC System, Agilent, Santa Clara, CA, USA), using a Luna 5 μm C18(2) 100 Å (250 × 10 mm) column (Phenomenex, Torrance, CA, USA) at 4.7 mL/min. The solvent systems used were A (H_2O with 0.1% TFA) and B (CH_3CN with 0.1% TFA). For separation, a linear gradient of 5–95% B in 45 min was applied and the detection was done at 214 nm and 254 nm.

2.4. Evaluation of peptide-Hsp90 interaction using colocalization in HCC cell line

Colocalization experiments were performed by conjugating biotin fluorophore to the linear peptide cargo (NovoPro Biosciences, Inc., Shanghai, China). HepG2 cells (3×10^5) were seeded into a 6-well plate overnight; each well contained a sterile coverslip for cells to attached onto. Medium was then removed, and cells washed three times with 1 × Phosphate-buffered saline (PBS) before fixing with 2% paraformaldehyde for 15 min at room temperature. After fixing, cells were washed twice with 1 × PBS, and permeabilized with 0.1% Triton X-100 for 15 min, followed by three washes with 1 × PBS. To reduce non-specific binding, 3% Bovine serum albumin (BSA) was added for one hour, followed by three washes with 1 × PBS. Biotin-labelled linear peptide and Hsp90 primary antibody (cat# sc-59577, Santa Cruz Biotechnology, Dallas, TX, USA) were co-incubated at 4 °C overnight, then washed three times with PBS before addition of Alexa Fluor™594-Streptavidin secondary antibody (cat# S11227, Invitrogen, Waltham, MA, USA) and goat anti-mouse Alexa Fluor™488 secondary antibody (cat# A-11029, Invitrogen, Waltham, MA, USA) to incubate for one hour at room temperature. After washing three times with 1 × PBS, cells were stained with DAPI (cat# D21490, Invitrogen, Waltham, MA, USA) for 15 min at room temperature. Cell monolayers were washed three times with 1 × PBS before the coverslips were sealed and observed under fluorescence microscope (Axio Observer Z1, Zeiss, Oberkochen, Germany).

2.5. Circular dichroism (CD) analysis of peptide and peptidomimetics

The circular dichroism (CD) profiles of the peptide and peptidomimetics in various environments were obtained by acquiring the spectra on a Jasco J-1500 spectrophotometer (Tokyo, Japan), using a 0.2-mm pathlength quartz cell (Hellma Analytics, Munich, Germany). MilliQ water or aqueous 2,2,2-trifluoroethanol (TFE, from Merck, Darmstadt, Germany) was used as solvent. The measurements were performed at 25 °C, and 16–32 scans were acquired.

2.6. Temperature stability studies of peptide and peptidomimetics

Peptides and peptidomimetics (2 mg each) were dissolved in 800 μL of PBS (1 × PBS, pH 7.4) and incubated at 80 °C in a preheated hot box. Samples (90 μL) were taken at different time points post-incubation (0, 2, 4, 8, 12 and 24 h). The samples were then mixed with 90 μL of solvent cocktail containing HPLC H_2O/TFA/CH_3CN (94.8:0.2:5 v/v/v) and filtered using 0.45-micron filter prior to HPLC injection. The peptides were analyzed by RP-HPLC 1260 Infinity II LC System (Agilent, Santa Clara, CA, USA) using a Luna 5 μm C18 (2) 100 Å (250 × 4.6 mm) column (Phenomenex, Torrance, CA, USA) at a flow rate of 1 mL/min using a linear gradient of acetonitrile from 5% to 50% in 15 min using ultraviolet (UV) detector at 214 nm and 254 nm. The solvent systems used was (i) HPLC grade water with 0.1% TFA and (ii) acetonitrile with 0.1% TFA.

2.7. In vitro binding of peptide and peptidomimetics to Hsp90

The *in vitro* binding affinities of linear peptide and its peptidomimetics with the target Hsp90 were evaluated using a label free field effect biosensing (FEB) PPI detection technique. The experiment was performed using AGILE Device (Cardea, San Diego, CA, USA) by immobilizing/cross-linking the target protein (Hsp90, 500 nM) onto activated carboxyl group present on the graphene biosensor chip activated by 1-Ethyl-3-(3-dimethylamino propyl) carbodiimide

(EDC) and N-Hydroxysulfosuccinimide (sulfo-NHS) using a standard protocol [35]. Each cycle of the experiment includes five repetitive steps starts with calibration using 1 × PBS (pH 7.4) followed by analyte association, dissociation, regeneration, and wash (5 times) consecutively. About ten different peptide/peptidomimetic analyte concentrations ranging from 2 μM to 1000 μM were prepared in sterile 1 × PBS (pH 7.4) for the binding studies with Hsp90. FEB measures the electric current through the graphene biosensor chip to which the binding target (Hsp90) is immobilized and the variations in current (I) at real-time upon interaction of peptide/peptidomimetic analytes were measured in the form of I-Response [35]. Each binding experiment was performed in three replicates, and the I-Responses from ten different analyte concentration points were exported from three transistors, averaged, and background noise recorded during calibration (PBS) was nullified. An automated Hill fit plot determining K_D value was generated. The analyte data points were exported to the statistical analysis software, GraphPad Prism 9.

2.8. In vitro competitive inhibition of Hsp90/Cdc37 PPI with peptides

We explored the biomolecular interaction between Hsp90 and its client protein, Cdc37, by immobilizing Hsp90 (500 nM) following the standard protocol using FEB technology [35]. About 10 concentrations of analyte protein, Cdc37, ranging from 0.4 nM to 200 nM were prepared in 1 × PBS (pH 7.4). The Cdc37 solution (25 μL), and 25 μL of the peptide solution (200 μM) were pre-incubated together with proper shaking at 4 °C for 1 h. Each binding experiment was performed in triplicates, and the I-Responses from the analyte concentration points were exported from three transistors, averaged, and background noise recorded during calibration (PBS) was nullified. An automated Hill fit plot determining K_D value was generated. The analyte data points were exported to the statistical analysis software, GraphPad Prism 9.

2.9. Co-immunoprecipitation

One million Huh7 cells were treated with 40 μM peptides for 16 h, then lysed with T-PER Tissue Protein Extraction Reagent (Pierce, Rockford, IL, USA). Lysed cells were then spin down, and 10% volume of the total supernatant prepared as the input sample, the remaining of the supernatant was used for co-immunoprecipitation (co-IP) assay. Primary Cdc37 antibody was added to the supernatant and spun for 3 h at 4 °C, then 25 μL protein A/G PLUS-Agarose (cat# sc-2003, Santa Cruz Biotechnology, Dallas, TX) was added to the supernatant for another 3 h. Agarose beads were then washed with T-PER Tissue Protein Extraction Reagent for three times, then boiled for 10 min with 1 × NuPAGE™ LDS sample buffer (NP0007, Thermofisher, Waltham, MA). The samples were run then using the same conditions as described below for Western blotting using Hsp90 antibody.

2.10. Cell proliferation activity of peptides in HCC cell lines

Human HCC cell lines, HepG2 and Huh7 were obtained from American Type Culture Collection (ATCC, Manassas, VA, USA). HepG2 and Huh7 were cultured in Eagle's Minimum Essential Medium and Dulbecco's Modified Eagle's Medium (ATCC, Manassas, VA, USA), respectively. Both media were supplemented with 10% fetal bovine serum (FBS), 100 U/mL penicillin, and 100 μg/mL streptomycin (all supplements were obtained from Life Technologies (Carlsbad, CA, USA)). Cells were maintained at 37 °C in a humidified 5% CO_2 atmosphere.

Cell proliferation assays of the peptides against HCC cell lines (HepG2 and Huh7) were performed using 3-(4,5-dimethylthiazol-2-yl)− 2,5-diphenyltetrazolium (MTT) assay kits (cat# G4100, Promega, Woburn, MA, USA). Cells were seeded into 96-well plates at 1 × 10^5 and 1 × 10^3 cells per well for HepG2 and Huh7 respectively, overnight. Cells were then treated three times a day, for three days, with the desired concentrations of peptides. On each day, the first two doses were of 20 μM, given at three hours intervals, followed by third dose of 40 μM, for both cell lines, using the same amount of PBS as the control group for three days. On the fourth day, 15 μL of MTT solution was added to each well for a four-hour incubation at room temperature, followed by the addition of 100 μL Stop Solution for one hour at 37 °C. OD values at 570 nm were measured by SYNERGY-LX absorbance microplate reader (BioTek, Winooski, VT, USA). The IC_{50} values were calculated by nonlinear fit curves using GraphPad Prism 9.0 software.

2.11. Apoptosis analysis

HepG2 cells (1 million cells per well) and Huh7 cells (0.35 million cells per well) were seeded in 6-well plates separately overnight. They were then treated with 40 μM of each peptide or PBS as control for 16 h. All cells were then harvested, including both adherent cells and supernatant cells in the medium, and then pelleted and fixed with Fixation Buffer and washed with Permeabilization Solution (cat# 88–8824–00, Invitrogen, Waltham, MA, USA). Thereafter, activated caspase3-FITC antibody was added followed by washing with Permeabilization Solution and analysis by flow cytometry.

2.12. In vitro wound healing assay

Cell migration was assessed using the wound healing assay. Huh7 cells (3 × 10^5) were seeded in a 6-well plate and allowed to form a monolayer for 24 h. A wound was generated by scratching on the bottom of the well with a sterile 200 μL pipette tip. The wells were washed with 500 μL PBS to remove the detached cells. Fresh medium (500 μL, without FBS but with 200 μg/mL BSA) was added with the desired final concentrations of each peptide for 24 h. The plate was then washed with 500 μL PBS and gently shaken for 30 s. The areas surrounding the scratch were photographed under a light microscope (Nikon, Tokyo, Japan) at the time the wound was created (0 h) and at 48 h after.

2.13. Protein extraction and Western blotting

Total protein was extracted from cultured cells using the T-PER Tissue Protein Extraction Reagent (Pierce, Rockford, IL, USA), and protein concentration was determined with BCA Protein Assay Kit (Pierce, Rockford, IL, USA). Equal amounts of protein (20 μg) were electrophoresed on 4–12% polyacrylamide gels (Invitrogen, Carlsbad, CA, USA), and transferred onto polyvinylidene difluoride membranes, blocked with 5% non-fat milk for one hour, and probed with primary antibodies against MEK1/2 (cat# 9122) and p-MEK1/2 (s217/221, cat# 9154), Hsp90 (cat# 4877 S), Cdc37 (cat# 4793 S) (all antibodies from Cell Signaling, Danvers, MA, USA). Antibody against the internal control, GAPDH (cat# 60004–1-Ig) was from Proteintech (San Diego, CA, USA). The specific proteins were detected with fluorescent secondary antibody IRDYE 800CW goat anti-rabbit (cat# 926–32211, LI-COR Biotechnology, Lincoln, NE, USA) and IRDYE 680RD goat anti-mouse (cat# 926–68070, LI-COR Biotechnology, Lincoln, NE, USA). Band intensities were measured by Image Studio Lite 5.0 (LI-COR Biosciences, Lincoln, NE, USA).

2.14. Statistical analysis

Statistical analyses were performed using the statistical software GraphPad Prism 9.0. All data were presented as means ± SD. One-way analysis of variance (ANOVA) followed by Tukey's multiple

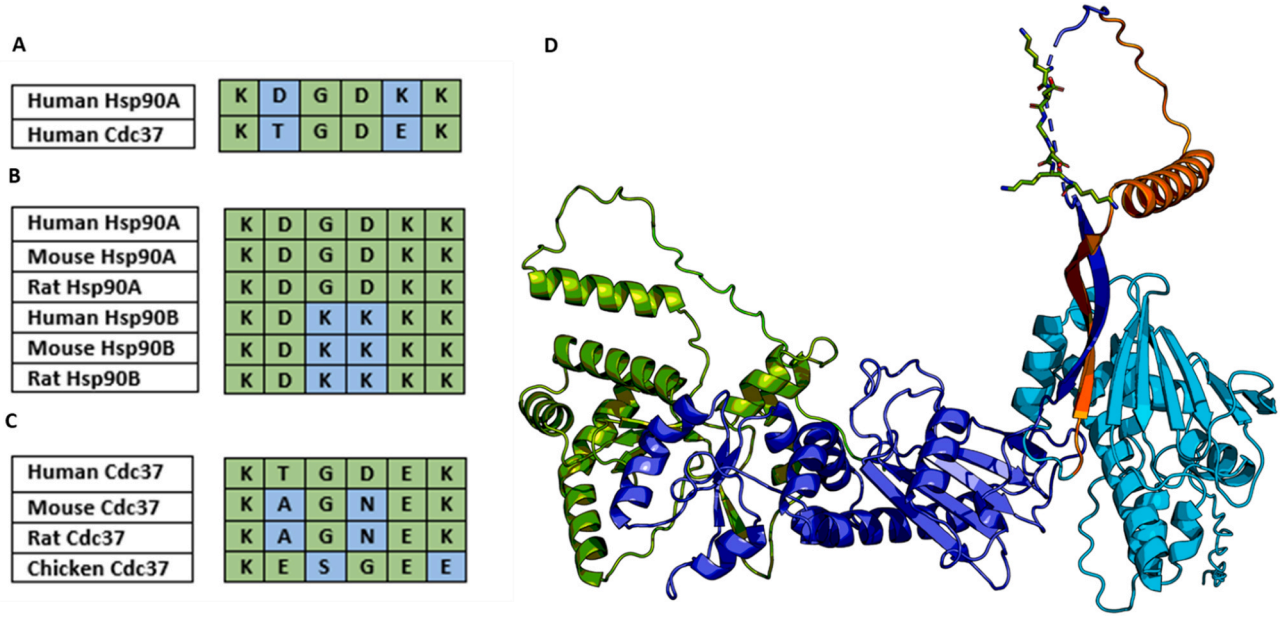

Fig. 1. Rational design of a peptide targeting Hsp90/Cdc37 PPI. **A.** Homology alignment between Hsp90 and Cdc37 results in the identification of a six amino acid sequence, KTGDEK, derived from the Cdc37 sequence. **B, C.** Sequence conservation of Hsp90A, Hsp90B, and Cdc37 among different species in evolution. **D.** Cdc37-derived peptide sequence, KTGDEK, shown as green sticks in the middle domain (MD) region of the three-dimensional (3D) predicted model of Hsp90 (Alpha Fold predicted model of human Hsp90: AF-P07900-F1) generated in PyMol (Schrodinger LLC) [38].

comparison tests was used to compare data with more than two groups.

3. Results and discussion

3.1. Design of a selective peptide targeting Hsp90/Cdc37 PPI

Recent studies have reported alternative ways to block the Hsp90/Cdc37 interaction effectively, either by targeting non-ATPase sites or its client Cdc37 binding site [10,36]. This offered a promising approach of rational design, optimization, and evaluation of specific peptide pharmacological leads to target Hsp90/Cdc37 PPI without affecting the highly conserved ATPase activity. Proteins habitually utilize complex network of PPIs to regulate cellular functions and biological processes. Thus, sequence alignment of the two proteins that are known to interact may reveal short homologous areas as potential candidates for the development of peptides that may have the potential to modulate their PPI [37]. We first identified such short homologous areas between Hsp90 and Cdc37 that may be used for targeting Hsp90/Cdc37 PPI. Using the LALIGN bioinformatics server, we identified a short six amino acid homology sequence, KTGDEK, between the interacting proteins Hsp90 and Cdc37 (Fig. 1. A). This hexapeptide sequence is found highly conserved among several species of Hsp90 and Cdc37 (Fig. 1. B, C).

3.2. Identification of peptide interaction sites on Hsp90

Hsp90 structurally exists as a homodimer that is characterized by ATPase activity and associations with co-chaperones. The Hsp90 monomer comprises three critical domains: (i) N-terminal domain (NTD), (ii) middle domain (MD), and (iii) C-terminal domain (CTD) [10]. The NTD contains the highly conserved ATP-binding domain intended to drive the conformation cycle of Hsp90 *via* ATP hydrolysis; the MD primarily acts as a binding/PPI site for client proteins and co-chaperones such as Cdc37; and the CTD is predominantly involved in the Hsp90 dimerization process to form the fully functional Hsp90 enzyme [39]. The NTD and MD are connected *via* a flexible, charged linker portion that offers flexibility to Hsp90 during ATP-mediated conformational shifts (Fig. 2). For example, the binding of ATP to the NTD induces a conformational shift of Hsp90 from an open to a closed conformation [10,39].

We performed molecular docking of the hexapeptide, KTGDEK, with its receptor protein Hsp90 in HPEPDOCK2.0 web server [28] to investigate the binding conformations, orientations, and binding mode of the peptide with Hsp90. Additionally, we used the Chou & Fasman secondary structure prediction to investigate the secondary structure of the peptide [31]. The docking server uses hierarchical flexible peptide docking algorithm as a scoring function to compare different peptide conformations [28]. We first performed a global search around the full protein to obtain the putative binding orientation of the peptide and selected the top peptide conformation (docking score −105.60) out of 10 best poses generated from HPEPDOCK2.0. HPEP docking offers flexibility to peptide without running any prolonged simulations. The hexapeptide can be accommodated in a binding pocket formed by the helices of the MD devoted to co-chaperones binding to Hsp90, and it is stabilized by seven hydrogen bonds calculated with a cutoff value of < 3.4 Å, formed between the hexapeptide and Thr298, Arg299, Lys294, Asp303, and Glu311 of Hsp90 (Fig. 3).

Peptide-protein docking is challenging due to the inherent flexibility of linear peptides. The conformational space of a peptide grows exponentially with the number of freely-rotating bonds [40]. Therefore, we also did a site/residue-specific docking of the hexapeptide with Hsp90 by specifying the binding residues based on the rational design. The top peptide conformation was selected out of 10 generated poses based on docking energy and exported into PyMol (Schrodinger LLC). The hexapeptide aligns perfectly with its homologous sequence found in the MD of Hsp90 with a docking score of − 51.29. The interaction was stabilized by two hydrogen bonds calculated with a cutoff value of < 3.4 Å between the hexapeptide and Asp271 and Lys276 of the Hsp90 MD (Fig. 4).

Both global and site/residue-specific docking analyses confirmed that the hexapeptide docked to the MD domain of Hsp90, which is a binding site for co-chaperones, and validated our rational design strategy.

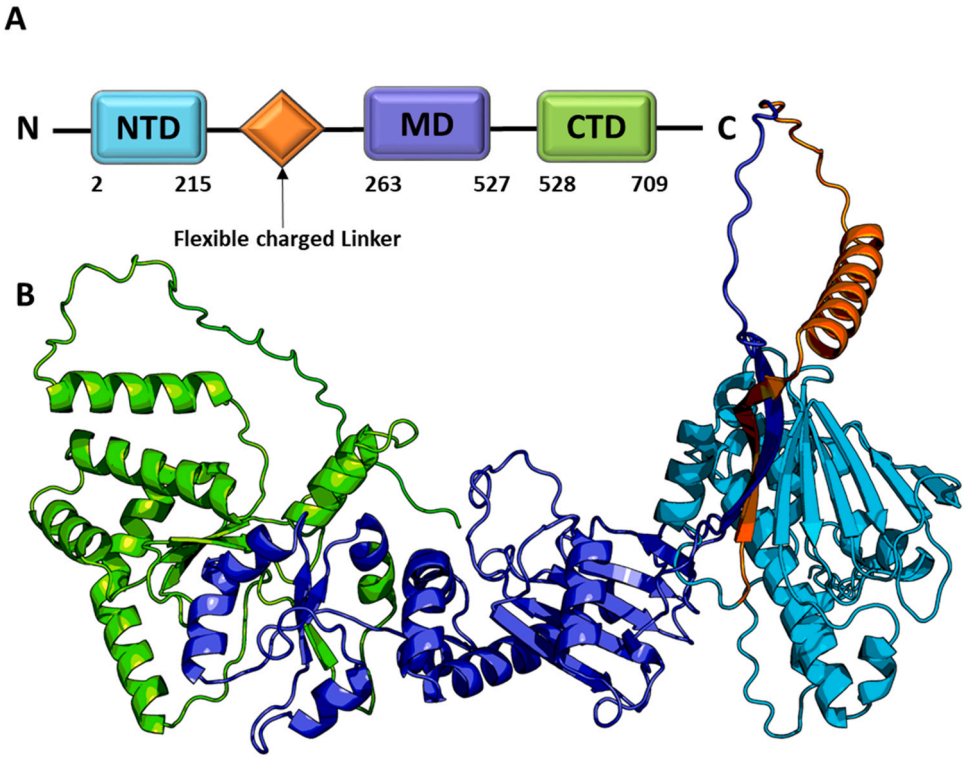

Fig. 2. Alpha Fold predicted 3D model of human Hsp90 with its domains (AF-P07900-F1). **A**. Hsp90 domain structures (i) N-terminal domain (NTD, cyan), (ii) middle domain (MD, purple), (iii) C-terminal domain (CTD, green), and a flexible charged linker (orange) connecting NTD and MD. **B.** Colored cartoon representation of Hsp90 domains. NTD shown in cyan, MD in purple, CTD in green, and the flexible charged linker in orange. The Hsp90 3D figure was generated using PyMol (Schrodinger LLC) [38].

3.3. Hexapeptide colocalized with Hsp90 in HCC cell line

Next, we synthesized the hexapeptide, KTGDEK, and conjugated it to the CPP TAT (YGRKKRRQRRR) to allow cell entry. To validate the cellular localization of KTGDEK, and its potential co-localization with Hsp90 in HCC cells, we labelled KTGDEK-TAT with the fluorescent biotin dye. Immunofluorescence staining performed in HepG2 cells showed that the biotin-labeled peptide localized within the cytoplasm of HepG2 cells (red signal, Fig. 5). Additionally, it co-localized with its target protein Hsp90 (green signal in the cytoplasm), as shown in the merged image (yellow signal in the cytoplasm). DAPI staining showed location of cellular nuclei (blue signal, Fig. 5).

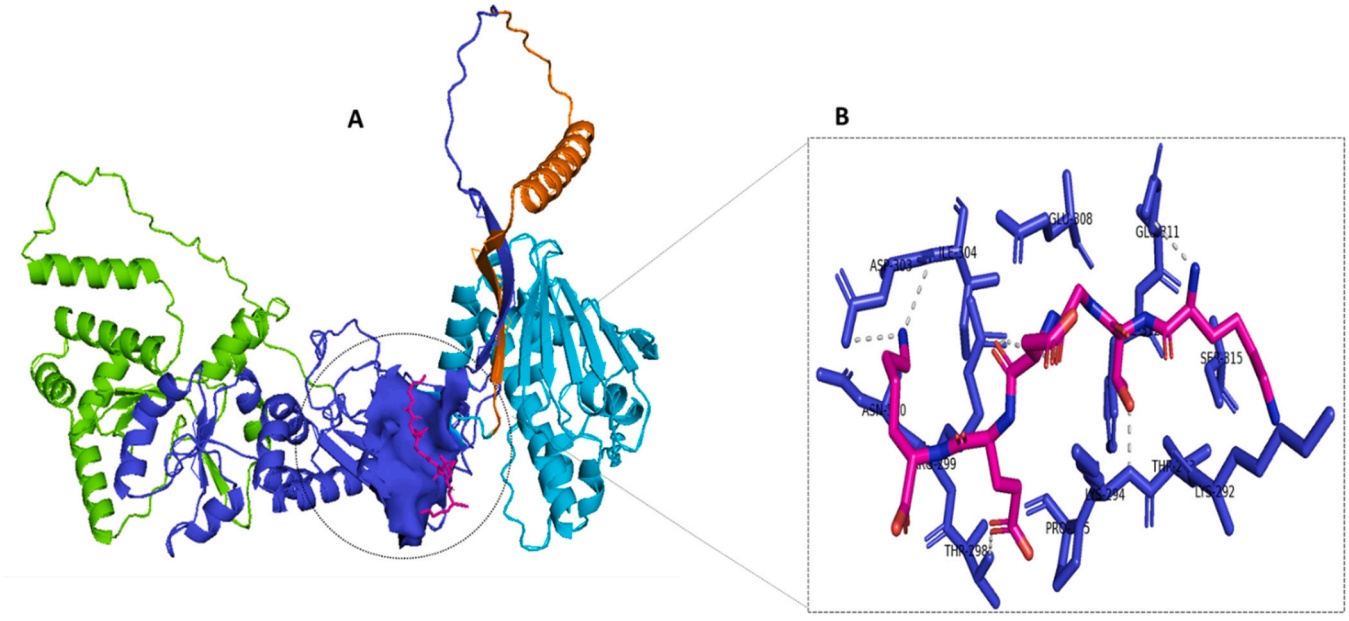

Fig. 3. Global docking of hexapeptide to Hsp90 based on HPEPDOCK2.0. **A.** Colored cartoon representation of Hsp90 domains with the hexapeptide binding site as a blue surface. Peptide is shown as magenta sticks. **B.** Magnified view of hexapeptide (magenta sticks) binding with interacting amino acid residues (blue sticks) on the MD of Hsp90. Hydrogen bonds calculated with a cutoff value of < 3.4 Å between the hexapeptide and the MD amino acids are displayed as grey dotted lines (Alpha Fold predicted model: AF-P07900-F1). The 3D figure was generated using PyMol (Schrodinger LLC) [38].

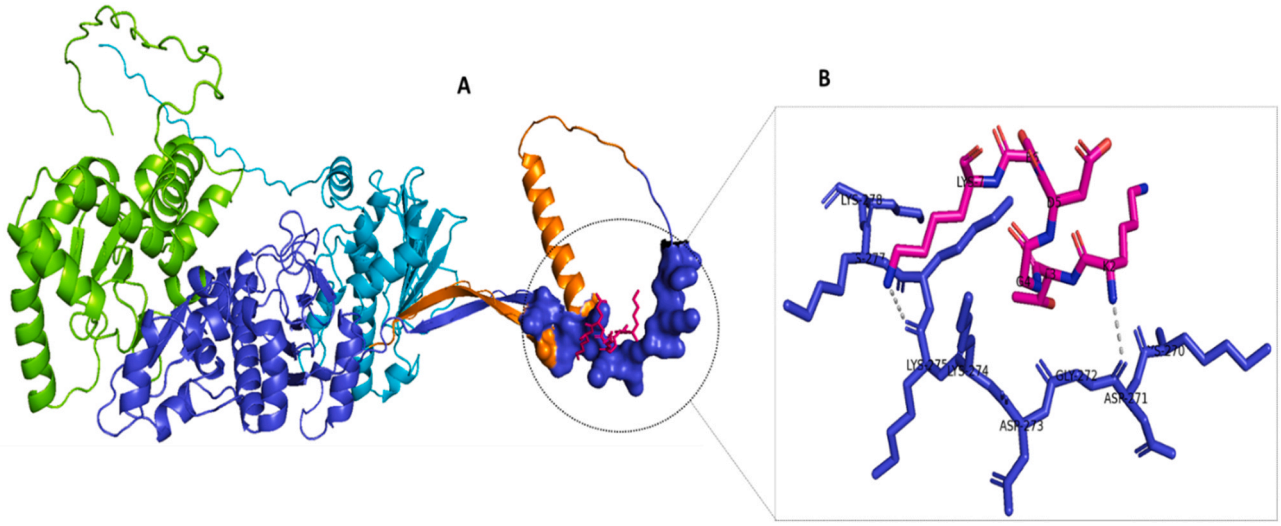

Fig. 4. Site/residue-specific docking of hexapeptide to Hsp90 based on HPEPDOCK2.0. **A.** Colored cartoon representation of Hsp90 domains with the peptide binding site as a blue surface. Peptide is shown as magenta sticks. **B.** Magnified view of hexapeptide (magenta sticks) binding to Hsp90 MD amino acid residues (blue sticks). Hydrogen bonds calculated with a cutoff value of < 3.4 Å between the peptide and MD amino acids are displayed as grey dotted lines (Alpha Fold predicted model: AF-P07900-F1). The 3D figure was generated using PyMol (Schrodinger LLC) [38].

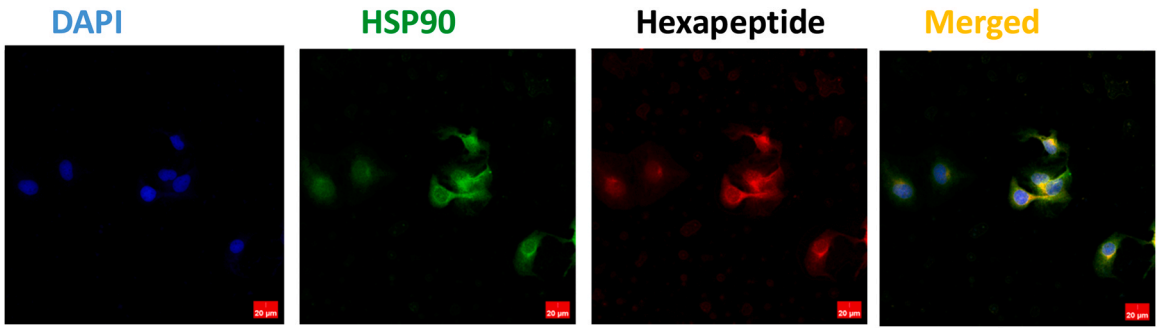

Fig. 5. Colocalization of Hsp90 and hexapeptide in HepG2 cells by immunofluorescence. Red scale bar represents 20 μM.

3.4. Generation of peptidomimetic library

Linear peptides may be used to design peptidomimetics by chemical modifications to transform them into more 'drug-like' molecules; this is possible due to the peptidomimetics adopting bioactive conformations [21]. Cyclization of parent linear peptides can circumvent their therapeutic disadvantages by improving their stability and target binding efficacy [22,23,33,41,42]. In some cases, the conformationally constrained cyclic peptides may lead to reduced bioactivity. Therefore, we designed a peptidomimetic library to screen for bioactive modified peptides of KTGDEK, consisting of two pre-cyclic and two cyclic peptidomimetics preserving the amino acid residues, KTGDEK. To perform the cyclization, an additional lysine residue carrying the orthogonal side-chain 4-methyltrityl (Mtt) protective group was conjugated to the N-terminal, forming KTGDEK-K [34]. All the peptidomimetics bear the same primary sequence, KTGDEK, and differ only in the bridge size. We also preserved the two termini of the peptide to mimic the native protein structure. To ensure cell internalization the peptidomimetics were conjugated to TAT [43]. The position of cyclization was determined by parent hexapeptide sequence, thus excluding TAT. The resulting peptidomimetics library is shown in Table 1 and Fig. 6.

The purity of the peptidomimetics was assessed using RP-HPLC and their identity validated by MALDI-MS (Table 2; for full characterization, see Figs. S1-S5 and Table S1).

Table 1
Schematic representation of the peptidomimetics library composed of the bioactive peptide cargo (green color), lysine residue for cross-linking (red color) and short Gly-Gly spacer (black color) to conjugate with TAT sequence (blue color).

Peptide Chemistry	*Sequence*	*Peptide Name*
Linear Pep	CH_3-CO-KTGDEK-K-GG-YGRKKRRQRRR-NH_2	CHP-026
Pre-Cyc-GA	CO-$(CH_2)_3$ -CO_2HKTGDEK -K-GG-YGRKKRRQRRR-NH_2	CHP-027
Pre-Cyc-SA	CO-$(CH_2)_2$ -CO_2H KTGDEK -K-GG-YGRKKRRQRRR-NH_2	CHP-028
Cyc-SA	CO-$(CH_2)_2$-CO-NH KTGDEK -K-GG-YGRKKRRQRRR-NH_2	CHP-029
Cyc-GA	CO-$(CH_2)_3$-CO-NH KTGDEK -K-GG-YGRKKRRQRRR-NH_2	CHP-030

Next, we tested the binding affinity of the modified peptidomimetics to Hsp90 *in vitro* using field-effect biosensing (FEB) technology, a label-free biophysical detection method which we reported previously [35]. The linear peptide CHP-026 showed the lowest binding affinity to Hsp90 with the highest K_D value of 342.5 μM. The cyclic peptides (Cyc-SA (CHP-029) and Cyc-GA (CHP-030) demonstrated improved binding to the target compared to the linear peptide with similar K_D values of 137.3 μM and 114.7 μM, respectively. Remarkably, the pre-cyclic peptidomimetics (Pre-Cyc-GA (CHP-027)

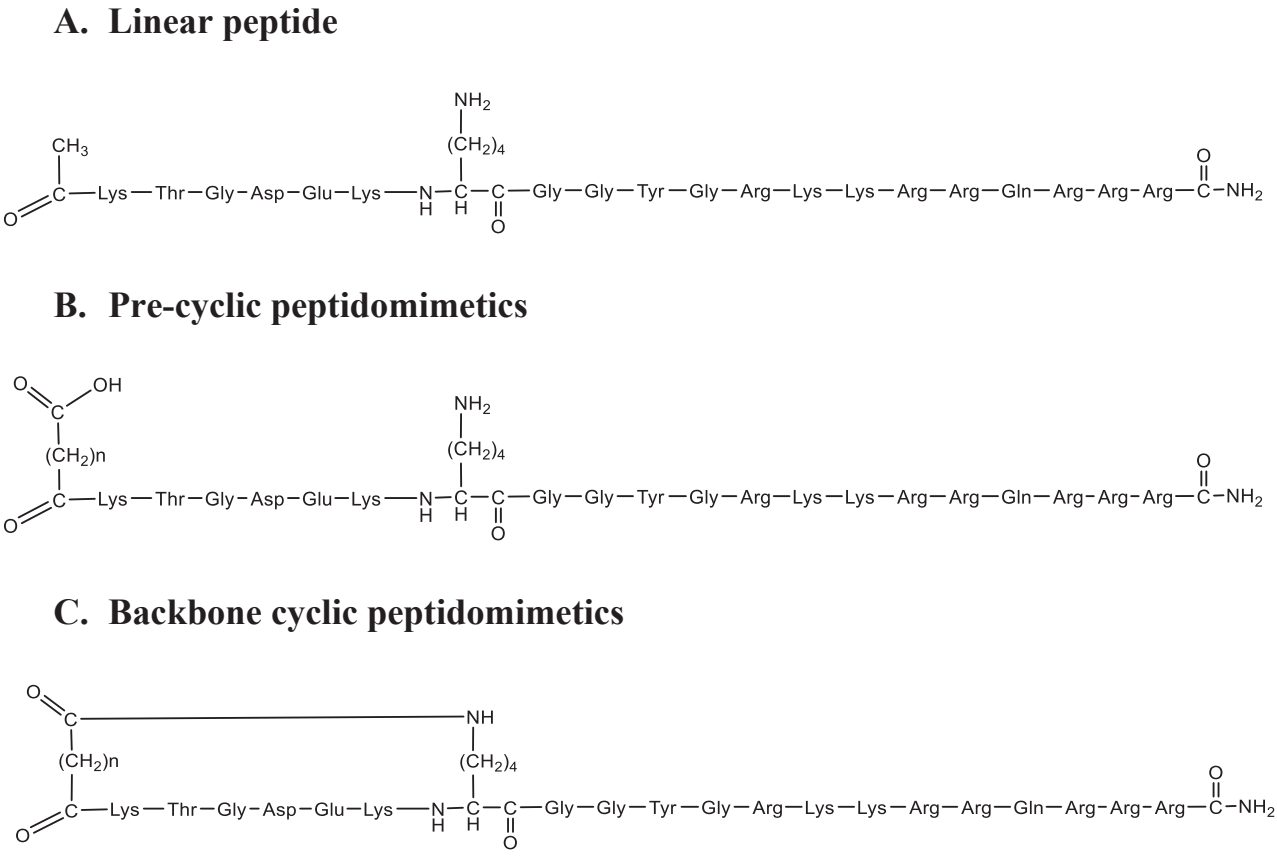

Fig. 6. Chemical structures of the peptidomimetics library. **A.** Linear peptide (CHP-026); **B.** Pre-cyclic peptidomimetics (CHP-027 and CHP-028); and **C.** Cyclic peptidomimetics (CHP-029 and CHP-030).

and Pre-Cyc-SA (CHP-028)) exhibited the highest binding affinities to Hsp90 with lowest K_D values of 30.03 μM and 16.40 μM, respectively. Overall, the chemical modification added a conformational constrain to the linear peptide, thereby enhancing the target binding affinity. The enhancement of binding affinity shown by the pre-cyclic and cyclic peptidomimetics highlights the validity of the chemical approach of restricting the peptide conformation to enhance target binding affinity. On the other hand, the enhanced conformational constrain present in the cyclic peptides (CHP-029 and CHP-030) may lead to reduced bioactivity (Table 3, Fig. 7).

3.5. Identification of peptidomimetic interaction sites on Hsp90

Next, we used the HPEPDOCK2.0 web server to perform molecular docking of the cargo of the pre-cyclic peptidomimetic with the highest binding affinity (CHP-028) with its receptor protein Hsp90 [28], as we did previously with the parent hexapeptide. The docking results showed that the pre-cyclic peptidomimetic has a docking score of about − 105.60, and that it is stabilized by seven hydrogen bonds with residues Thr298, Arg299, Lys 294, Asp303, and Glu311 of Hsp90 (Fig. 8). Both parent hexapeptide, CHP-026, and CHP-028

Table 3
In vitro binding K_D values of the peptidomimetics to their target Hsp90.

Peptide code	K_D (μM)	R^2 Value	Peptide name
CHP-026	342.50 ± 25.31	0.99	Linear Pep
CHP-027	30.03 ± 5.44	0.99	Pre-Cyc-GA
CHP-028	16.40 ± 3.44	0.99	Pre-Cyc-SA
CHP-029	137.30 ± 24.30	0.99	Cyc-SA
CHP-030	114.70 ± 54.54	0.99	Cyc-GA

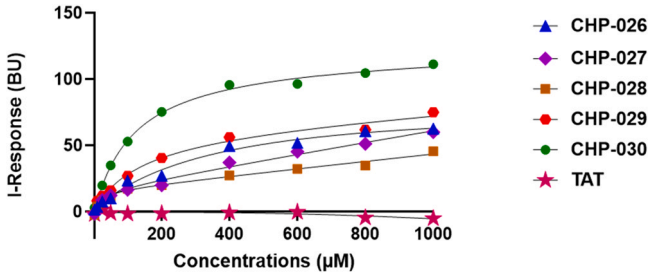

Fig. 7. Binding interactions between peptides and the target Hsp90.

Table 2
The HPLC and MALDI-MS characterization profile of peptidomimetics library. 'n' refers to the number of methylenes in the alkyl spacer.

Peptide code	n	*Bridge size*	*Ring size*	*Calculated MH^+ (g/mol)*	*Observed MH^+ (M/Z)*	*Purity HPLC (%)*	*Peptide name*
CHP-026	-	-	NA	2501.88	2507.52	100.00	Linear Pep
CHP-027	3	-	NA	2573.85	2578.95	100.00	Pre-Cyc-GA
CHP-028	2	-	NA	2559.85	2564.78	100.00	Pre-Cyc-SA
CHP-029	2	9	41	2541.85	2546.95	100.00	Cyc-SA
CHP-030	3	10	42	2555.85	2560.86	100.00	Cyc-GA

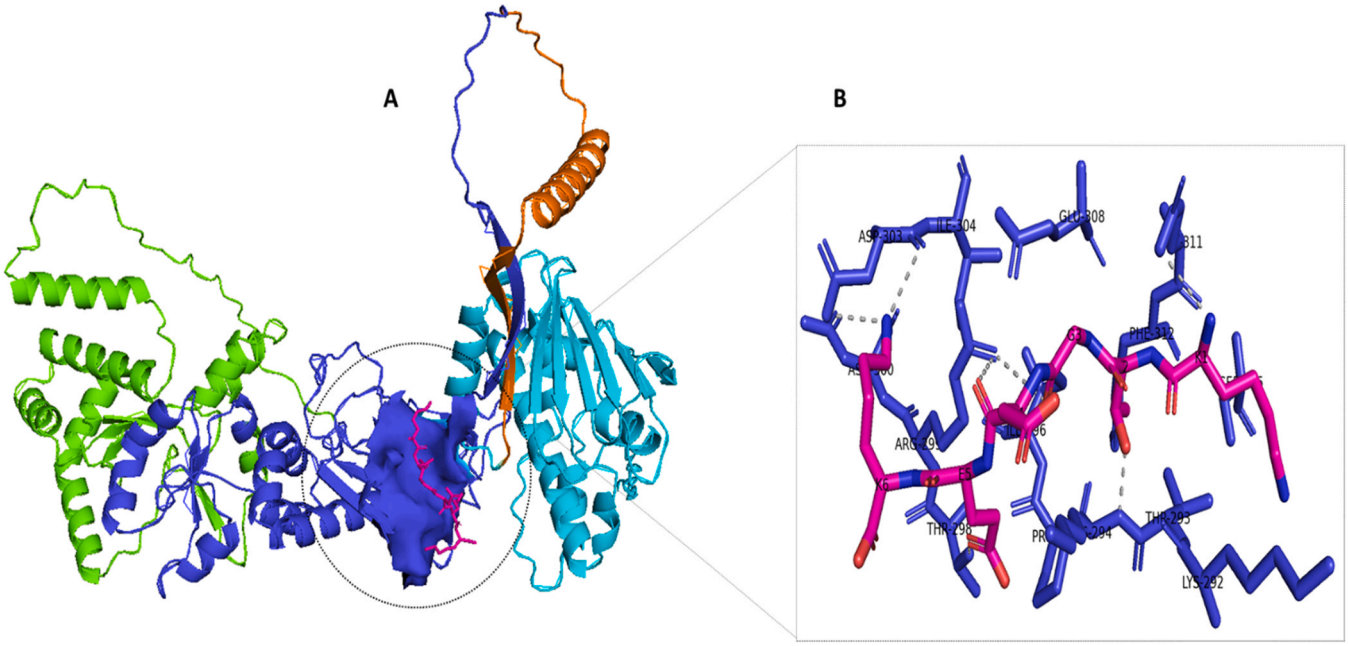

Fig. 8. Global docking of cargo peptide of CHP-028 to Hsp90 based on HPEPDOCK2.0. **A.** Colored cartoon representation of Hsp90 domains with the peptide binding site as a blue surface. Cargo peptide of CHP-028 is shown as magenta sticks. **B.** Magnified view of CHP-028 peptide (magenta sticks) binding with the interacting amino acid residues (blue sticks) of Hsp90 MD. Hydrogen bonds calculated with a cutoff value of < 3.4 Å between CHP-028 cargo peptide and MD amino acids are displayed as grey dotted lines (Alpha Fold predicted model: AF-P07900-F1). The 3D figure was generated using PyMol (Schrodinger LLC) [38].

Table 4
Site/residue-specific docking profile of linear and pre-cyclic peptidomimetics with Hsp90.

Peptide names	*Peptide chemistry*	*Docking score*	*Hydrogen bonds (< 3.4 A°)*	*Residues involved in Hydrogen bond*
CHP-026	Linear Pep	-51.29	2	Asp271, Lys276
CHP-028	Pre-Cyc-SA	-71.54	5	Asp273, Lys275, Lys277

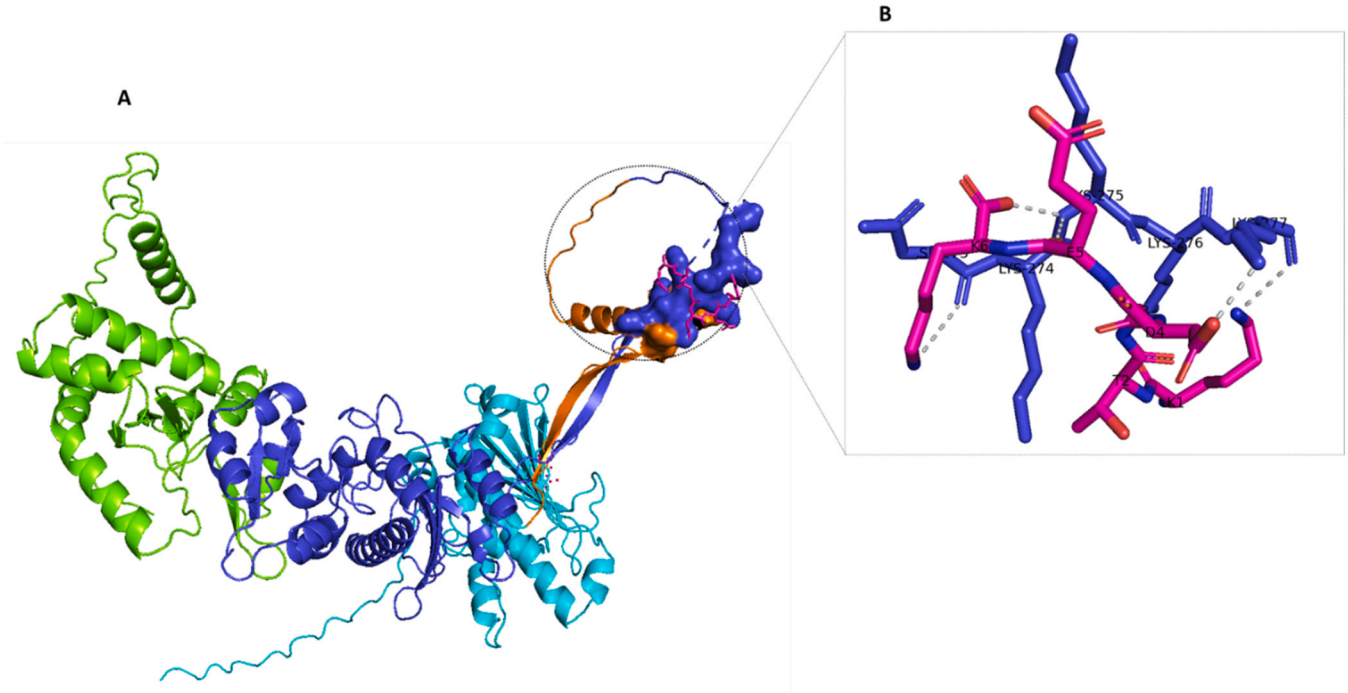

Fig. 9. Site/residue-specific docking of CHP-028 cargo peptide to Hsp90 based on HPEPDOCK2.0. **A.** Colored cartoon representation of Hsp90 domains with the peptide binding site as a blue surface. Cargo peptide of CHP-028 is shown as magenta sticks. **B.** Magnified view of CHP-028 cargo peptide (magenta sticks) binding to Hsp90 MD amino acid residues (blue sticks). Hydrogen bonds calculated with a cutoff value of < 3.4 Å between the cargo peptide and MD amino acids are displayed as grey dotted lines (Alpha Fold predicted model: AF-P07900-F1). The 3D figure was generated using PyMol (Schrodinger LLC) [38].

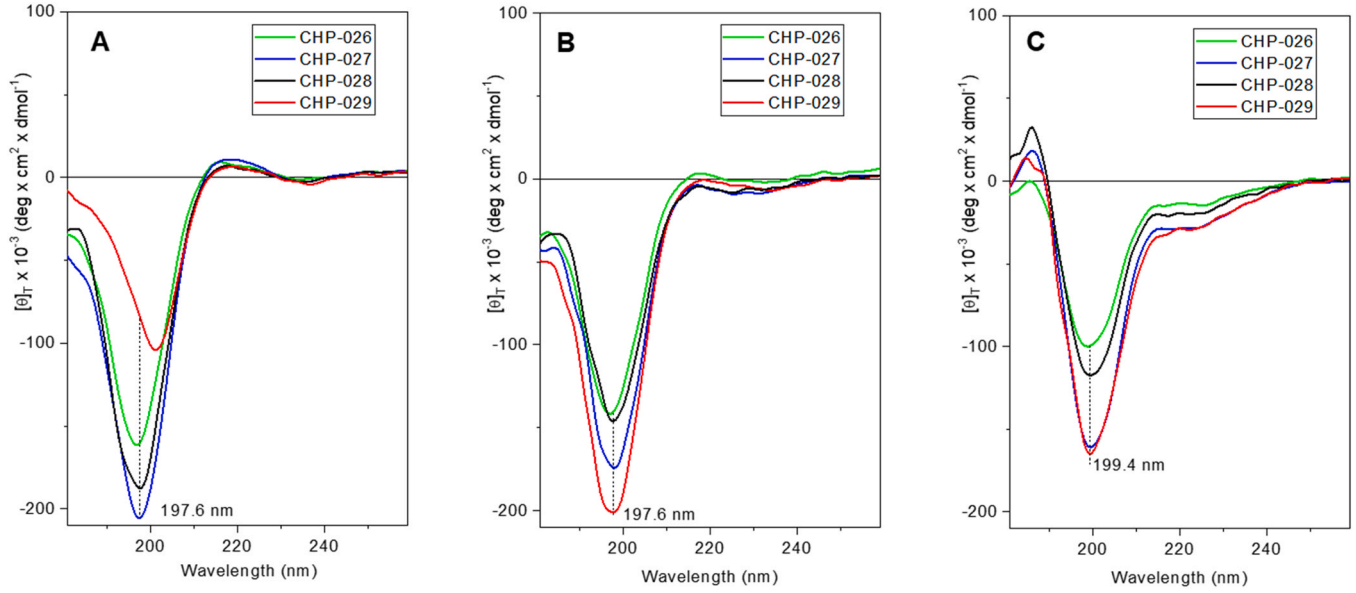

Fig. 10. CD profiles acquired for the linear (CHP-026), pre-cyclic (CHP-027, CHP-028), and cyclic (CHP-029) peptides in pure water (**A**), and in the presence of 10% TFE (**B**) or 40% TFE (**C**). Peptide concentration: 0.5 mM. The position of the negative dichroic band, corresponding to the parallel component of the π→π* electronic transition, is reported.

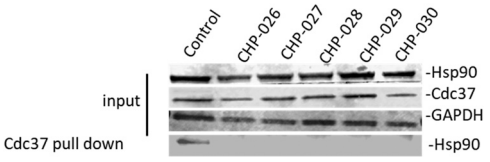

Fig. 11. Peptidomimetics disrupt Hsp90/Cdc37 interaction in HCC cells. Huh7 cells were treated with 40 μM of each peptidomimetic for 16 h. Hsp90/Cdc37 complexes in the cell lysates were then pulled down by anti-Cdc37 antibody. Anti-Hsp90 antibody was used to detect the presence of Hsp90 protein pulled-down complexes. The lysates were used to detect Hsp90, Cdc37, and GAPDH (loading control).

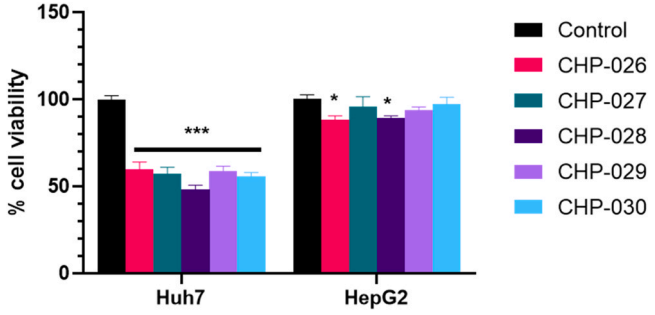

Fig. 13. Cell viability assay using peptidomimetics to validate their bioactivity in HCC cell lines (Huh7 and HepG2). Peptidomimetics inhibit HCC cells proliferation. Huh7 and HepG2 cells were treated three times a day, for three days, with the desired concentrations of peptides. On each day, the first two doses (20 μM) were given at three hours intervals, followed by third dose (40 μM) for both cell lines, using the same amount of PBS for the control group. Data expressed as mean ± standard deviation; *P < 0.05, ***P < 0.001 when compared to untreated control cells; n = 5.

were shown to have similar docking score of ∼ − 105, and to accommodate in the same binding pocket formed by the helices of the MD that is devoted to co-chaperones binding in Hsp90 (Figs. 3 and 8).

Next, a site/residue specific docking was also performed by specifying the binding residues. The cargo of the conformationally constrained pre-cyclic peptidomimetic, CHP-028, showed enhanced binding affinity compared to the linear counterpart CHP-026, with docking score − 71.54 and − 51.29 respectively. It was stabilized by five hydrogen bonds between the CHP-028 cargo peptide and Asp273, Lys275, and Lys277 of Hsp90 MD (Table 4, Fig. 9).

3.6. Circular dichroism analysis of peptides

Circular dichroism (CD) is a useful tool to monitor the secondary structure of proteins and peptides [44]. CD band positions are used

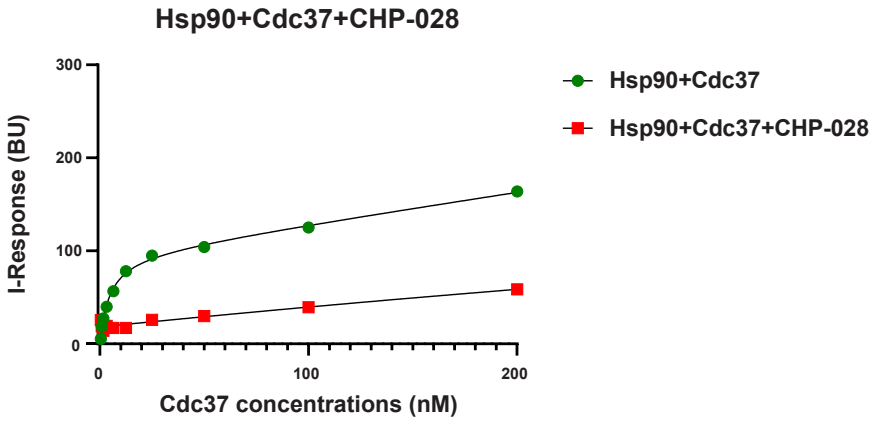

Fig. 12. *In vitro* binding association plots for Hsp90/Cdc37 interaction (green curve) and Hsp90/Cdc37 +CHP-028 competitive binding (red curve) generated using Graphpad Prism.

Table 5
In vitro binding K_D values of the Hsp90/Cdc37 interaction and Hsp90/Cdc37 + CHP-028 competitive binding.

Experiment Name	K_D Value (μM)	R^2 Value
Hsp90/Cdc37 interaction	0.004 ± 0.002	0.99
Hsp90/Cdc37 +CHP-028 competitive binding	2.78 ± 0.02	0.96

to identify the conformation adopted by macromolecules. In general, the CD spectrum of a peptide adopting an unordered structure features a negative band in the wavelength interval 190–200 nm, centered at about 195 nm, and a positive band at about 215 nm. All peptides display a CD profile of an unordered structure in water, with the typical two bands, one negative at about 198 nm and one positive at about 218 nm (Fig. 10. A) [45]. In both water and 10% 2,2,2-trifluoroethanol (TFE), the negative band falls at 197.6 nm for the pre-cyclic peptidomimetics. By increasing the amount of TFE to 40% to create a more hydrophobic environment, the band shifts to 199.4 nm (Fig. 10. C), suggesting a more structured conformation. However, the position of the negative band for the linear peptide always appears at a lower wavelength than that of its pre-cyclic analogs, meaning that its unordered conformation is resistant to perturbation by even a large amount of the structure-promoting solvent TFE. At the same time, by adding TFE, the small positive band centered at about 218 nm gradually becomes negative and centered at about 220 nm, and a small positive band at about 195 nm appears for all the investigated peptidomimetics. These changes in the CD profile are all diagnostic of a switch towards a more structured conformation, although the position of the main negative dichroic band, corresponding to the parallel component of the $\pi \rightarrow \pi^*$ electronic transition, never reaches the canonical value for a helical structure, which is above 200 nm (205–208 nm) [45]. The stronger preference of the linear peptide towards an unordered 3D-structure is confirmed by the persistent presence of the positive band at about 218 nm even in 10% TFE. Moreover, the positive band at about 195 nm does not appear for the linear peptide regardless of experimental conditions.

The presence of an additional, N-terminal amide bond in the pre-cyclic and cyclic peptidomimetics appears to promote the onset of a more structured conformation, which may facilitate their interaction with Hsp90. This is evidenced by the increasing *R* ratio between the two negative maxima ($R = [\theta]_{199}/[\theta]_{222}$) in 40% TFE, from 0.13 for the linear peptide, to 0.17 for the pre-cyclic peptidomimetic CHP-028, and to 0.18 for both peptidomimetics CHP-027 and CHP-029. Values of *R* that are far below 0.3 confirm the presence of a modest percentage of structured conformations for all peptide tested, which is particularly low for the linear peptide, even in the structure-supporting experimental condition of 40% TFE. Taken together, the CD data suggest that: (i) The linear peptidomimetic adopts an unordered conformation in all the environments tested. (ii) All tested peptidomimetics assume an unordered structure in water. (iii) The pre-cyclic peptidomimetics switch towards a slightly more structured conformation in 40% TFE, which is the most hydrophobic environment tested, and is the model environment that most closely resembles that for a peptide-protein interaction. However, the canonical band position and *R* value for a helical structure were not reached. (iv) The cyclic peptidomimetic CHP-029 appears to undergo more pronounced conformational changes in response to solvent variations than the linear and pre-cyclic peptides, especially in the presence of different amount of TFE (Figs. S6-S10). This observation may partially explain the enhanced binding affinity of the pre-cyclic peptidomimetics compared to the cyclic CHP-029, since its conformational indecision may slow down its binding to the target.

3.7. Temperature stability studies of peptidomimetics

Based on the binding affinity results, temperature stability studies were performed on the molecules with the highest binding affinity CHP-026 (the linear peptide), CHP-028 (pre-cyclic peptido-

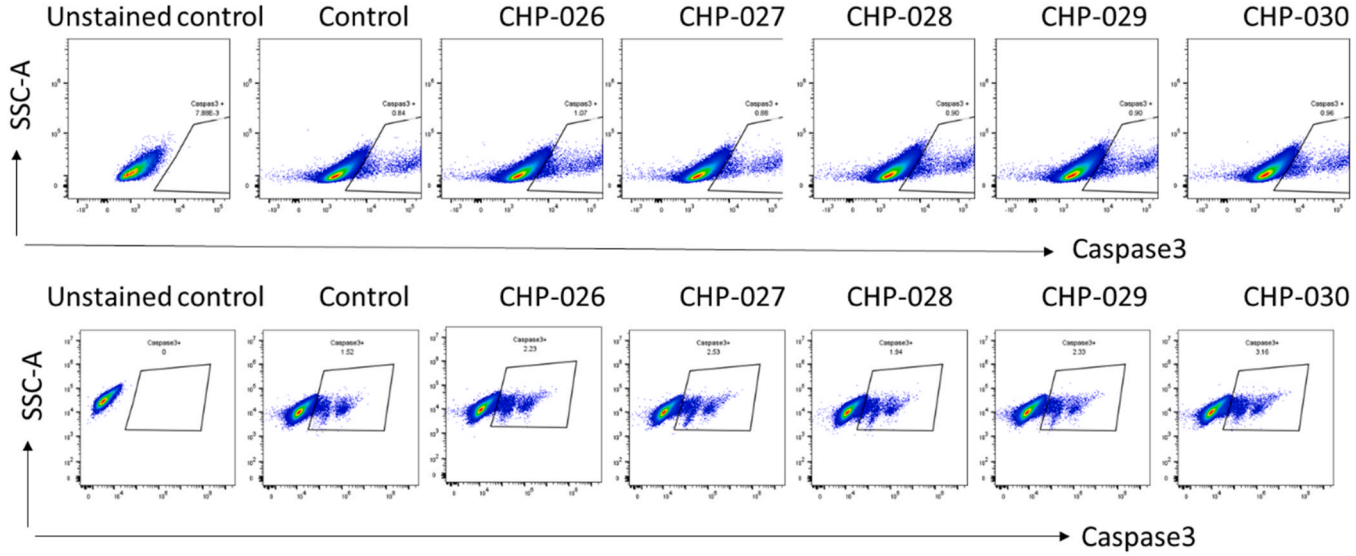

Fig. 14. Peptidomimetics enhanced HCC cells apoptosis. HepG2 cells (upper panel) and Huh7 cells (bottom panel) were treated with peptides (40 μM) for 16 h, and apoptosis was analyzed based on caspase-3 level determined by flow cytometry. "Unstained control" refers to experiment done in the absence of antibodies; "Control" refers to untreated cells.

Table 6
Quantification of the percentage of caspase-3 positive cells in HepG2 and Huh7 cells.

% Cells with caspase-3	*Unstained control*	*Control*	*CHP-026*	*CHP-027*	*CHP-028*	*CHP-029*	*CHP-030*
HepG2	0	0.84	1.07	0.88	0.90	0.90	0.96
Huh7	0	1.52	2.23	2.53	1.94	2.33	3.16

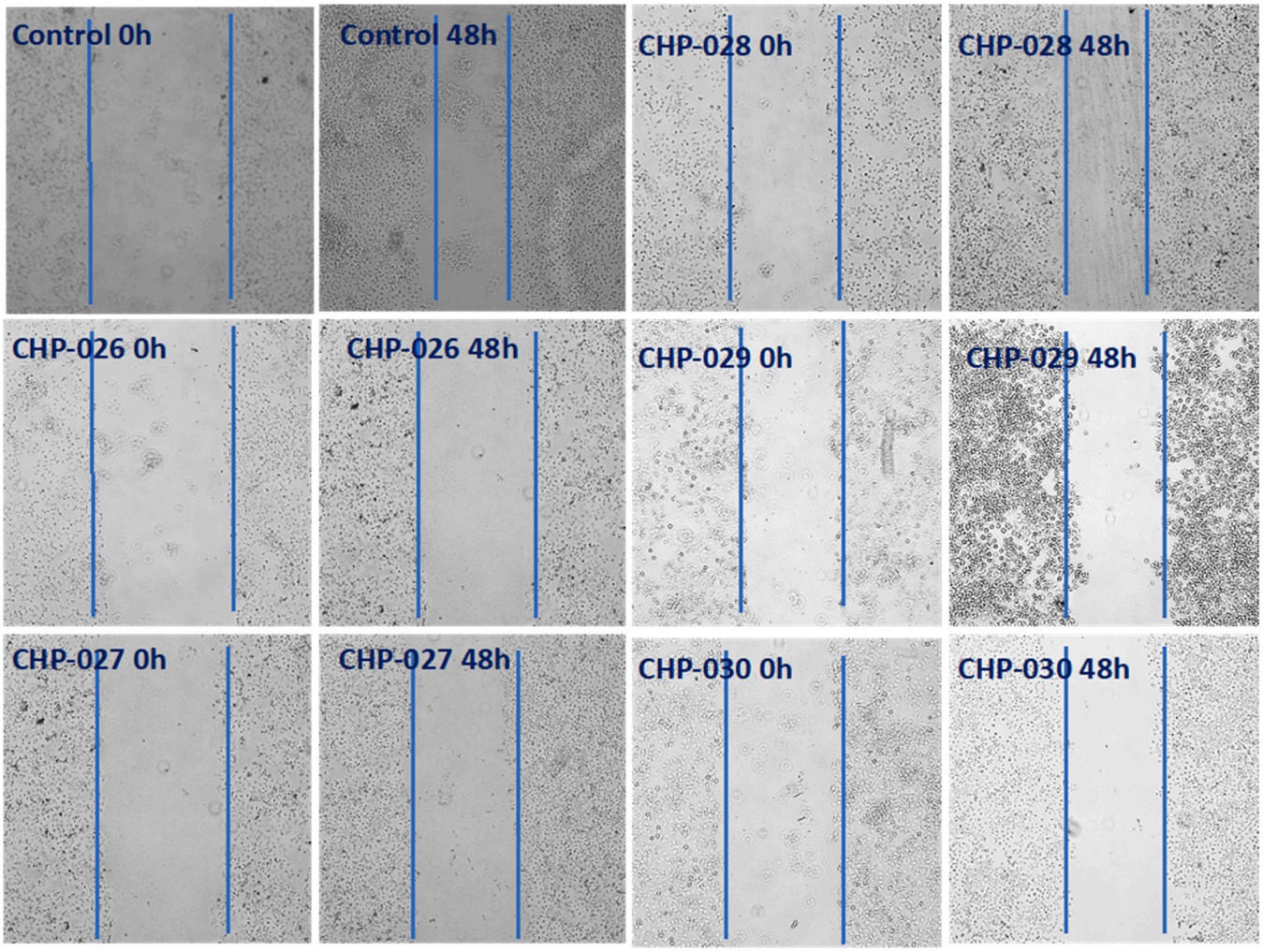

Fig. 15. Peptidomimetics (40 µM) inhibited Huh7 cell migration after treatment for 48 h. Untreated Huh7 cells were more efficient at closing the induced scratch wound than cells treated with the peptidomimetics.

mimetic), and CHP-029 (the cyclic peptidomimetic derived from CHP-028) at 80 °C. All three peptidomimetics were equally stable, as shown by their 100% HPLC purity profile devoid of any shift in the retention time (Table S2).

3.8. Peptidomimetics inhibit Hsp90/Cdc37 PPI in HCC cells

To verify that the peptidomimetics can disrupt Hsp90/Cdc37 PPI in HCC cells, we performed co-IP experiment using agarose beads linked to anti-Cdc37 antibody to pull down Hsp90/Cdc37 complexes in Huh7 cells that were treated with each peptidomimetic. Our results showed that Hsp90 was pulled down (and therefore detected) only in the untreated control cells but was not pulled down (undetected) in cells treated separately with each peptide (Fig. 11). The data suggest that each peptidomimetic can effectively disrupt the interaction of Hsp90/Cdc37 within the Huh7 cells.

3.9. In vitro Competitive Inhibition of Hsp90/Cdc37 PPI with CHP-028

Based on the FEB binding results of the peptidomimetics with their target Hsp90, Pre-Cyc-SA peptide (CHP-028) exhibited the highest binding affinity with a lowest K_D value of 16.40 µM. Therefore, next we performed a competitive study to evaluate if the peptide inhibits Hsp90/Cdc37 PPI. All experimental steps were monitored in real time and the K_D values were calculated by following the alterations in I-Response upon increasing analyte concentrations according to the standard protocol [35]. The K_D value for Hsp90/Cdc37 interaction was found to be 0.004 ± 0.002 µM, indicating a strong interaction between the target protein, Hsp90 and the analyte, Cdc37. To further validate the biophysical inhibition of Hsp90/Cdc37 PPI, a competitive inhibition study was done using the most biologically active peptidomimetic Pre-Cyc-SA (CHP-028). We determined that the K_D value for the interaction between Hsp90 and Cdc37 in the presence of CHP-028 was 2.78 ± 0.02 µM, which was significantly higher than the K_D value obtained for Hsp90/Cdc37 PPI (Fig. 12 and Table 5). Thus, competitive binding studies suggest that CHP-028 can effectively disrupt the interaction of Hsp90/Cdc37.

3.10. Peptidomimetics inhibit HCC cell proliferation in vitro

Having validated that the peptides inhibit Hsp90/Cdc37 interaction *in vitro,* we next wanted to validate their bioactivity by performing proliferation assay in two HCC cell lines, Huh7 and HepG2, both of which express Cdc37 and Hsp90 [46,47]. All peptidomimetics exhibited growth inhibitory activity in both HCC cell lines tested, with greater effects being seen in Huh7 cells. In Huh7 cells, Pre-Cyc-SA (CHP-028) showed the most potent growth inhibitory effect, causing about 50% cell kill compared to untreated cells. Both pre-cyclic derivatives (CHP-028 and CHP-027) were more potent than their cyclic or linear counterparts. This is consistent with our observation that they have the lower K_D values compared to the linear

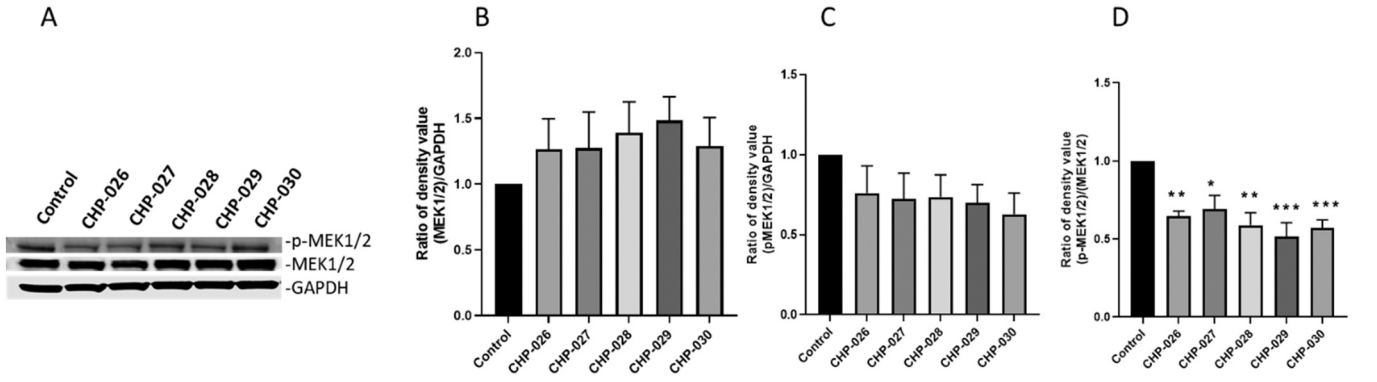

Fig. 16. Peptidomimetics inhibited downstream MEK1/2 signalling pathway of Hsp90/Cdc37 PPI in Huh7 cells. Cells were treated with peptidomimetic (40 μM) for 16 h, before cell proteins were extracted for Western blotting. GAPDH was used as the internal control. **A.** Western blot of MEK1/2 and p-MEK1/2; **B.** Densitometry analysis of (MEK1/2)/GAPDH ratio; **C.** Densitometry analysis of (p-MEK1/2)/GAPDH ratio; **D.** Ratio of normalized values of p-MEK1/2 and MEK1/2. Data are presented as Mean ± SEM, *p < 0.05, **P < 0.01, ***P < 0.001, n = 4.

and the cyclic derivatives. In HepG2 cells, Pre-Cyc-SA (CHP-028) caused a similar level of growth inhibition as the linear peptidomimetic, whereas other peptidomimetics did not elicit a significant growth inhibitory effect on HepG2 cells (Fig. 13).

This discrepancy between the two cell lines may be due to underlying differences in their genetic and/or molecular makeup. It has been reported that the CPP TAT sequence (YGRKKRRQRRR) may have growth-inducing properties in certain cancer cells [48–50]; this effect may confound the observations with the peptidomimetics that are conjugated with TAT. Specifically, TAT exerts proliferative effects on cells with epithelial morphology [50,51] and HepG2 cells have greater epithelial morphology and retain many metabolic functions like that of normal hepatocytes [52]. Detailed investigations into the effect of TAT, and the possible replacement with other CPPs may be warranted for further optimizations.

3.11. Peptidomimetics increase caspase-3 level in HCC cells

To further understand the mechanism underlying the anti-proliferative effects of the peptidomimetics, we assessed whether they induce apoptosis in HCC cells. Our data suggest that they cause a small increase in the percentage of caspase-3 positive cells in HepG2 cells, and a modest increase in Huh7 cells (Fig. 14, and Table 6), which may lead to increased apoptosis. Consistent with our cell proliferation data, Huh7 cells are more responsive to treatment with the peptidomimetics. The enhanced caspase-3 levels and apoptosis are in agreement with many reports that inhibitors of Hsp90/Cdc37 interaction induce apoptosis while inhibiting proliferation [53,54], making them a promising anti-tumor agent.

3.12. Peptidomimetics inhibit HCC cell migration

We further explored potential biological functions that may be affected by the peptidomimetics. Using the wound healing assay, we observed that Huh7 cells treated with the peptidomimetics decreased the ability of Huh7 cells to close the induced scratch (Fig. 15). Visual inspection of the scratched wound after 48 h showed that untreated Huh7 cells were able to migrate towards the centre of the wound more efficiently than treated cells. This suggest that the peptidomimetics slowed the migration of Huh7 cells. Consistent with our observations, Jin et al. found that 18b-glycyrrhetinic acid conjugated aminobenzothiazole derivatives of Hsp90/Cdc37 interaction disruptors inhibited human lung cancer cell migration as determined by similar wound healing assay [55], and also induced cell apoptosis, which we observed as well.

3.13. Peptidomimetics decreased phosphorylation of p-MEK1/2 in HCC cells

The interaction of Hsp90/Cdc37 leads to the downstream activation of multiple client protein kinases that subsequently mediate various cellular functions. To study the molecular impact resulting from treatment with the peptidomimetics, we detected the levels and phosphorylation status of a major client protein kinase, mitogen-activated protein kinase kinases 1 and 2 (MEK1/2), that is highly activated in HCC [56,57]. Treatment of Huh7 cells with the peptidomimetics (40 μM) for 16 h reduced phosphorylated MEK1/2 levels but not MEK1/2 levels, compared to untreated control (Fig. 16). Our results suggest that the peptidomimetics are bioactive and are able to inhibit the PPI between Hsp90/Cdc37, resulting in down-regulation of downstream phosphorylation of MEK1/2. Since the Raf/MEK/ERK signaling is activated in more than 50% of HCC, the ability to down-regulate one or more components of this pathway presents a feasible approach to controlling HCC cell growth. Subsequent detailed exploration of the effects of these peptides on the major downstream targets of Hsp90/Cdc37 will be required to fully understand their biological activities and impact on cancer cell growth.

4. Conclusion

In summary, we used a rational approach to successfully design a bioactive hexapeptide targeting Hsp90/Cdc37 PPI. By a stepwise strategy, we incorporated the bioactive peptide sequence into peptidomimetics with enhanced 'drug-like' properties to specifically target Hsp90/Cdc37 PPI. We demonstrated that the conformationally constrained pre-cyclic and cyclic peptidomimetics can bind the target protein with enhanced affinity. Moreover, *in silico* and *in vitro* experiments demonstrated that one pre-cyclic peptidomimetic, CHP-028, is the most bioactive compound when compared to its linear and cyclic counterparts. Conversely, the enhanced conformational constrain imposed on the cyclic peptidomimetics appears to limit their bioactivity. The pre-cyclic peptidomimetics also exhibited a greater anti-tumor efficacy against HCC cell lines, demonstrated by induction of HCC cell apoptosis and inhibition of HCC cell proliferation and migration. Our observations are consistent with reports on the anti-tumor properties of other classes of Hsp90 inhibitors. Finally, CHP-028 down-regulated the phosphorylation of MEK1/2, suggesting that it can target Hsp90/Cdc37 PPI within HCC cells to affect one of its major downstream signalling pathways in HCC. Overall, this comprehensive methodology of rational design, *in silico* evaluation, structural optimization and *in vitro* cell-based validation of 'drug-like' peptidomimetics against Hsp90/Cdc37 may offer innovative bioactive peptide tools to target HCC.

Author statement

Declaration of Generative AI and AI-assisted technologies in the writing process. During the preparation of this work the author(s) did not any AI-assisted technologies.

Declaration of Competing Interest

The authors declare no conflict of interest.

Acknowledgments

This research was supported by a grant from the Binational Science Foundation (BSF) to S.K.S. and N.Q., and by the CJ Huang Foundation to M.S.C., M.T., and H.Z. The authors would like to thank Yoav Luxembourg for his generous support. We also wish to acknowledge the help rendered by Avraham Samson for helpful guidance in docking analysis, and Moshe Dessau for sharing his computational knowledge in Structural Biology. M.D.Z. gratefully acknowledges funding by the Italian Ministry of University and Research (PRIN Project 2020833Y75).

Appendix A. Supporting information

Supplementary data associated with this article can be found in the online version at doi:10.1016/j.csbj.2023.05.023.

References

[1] Sung H, et al. Global cancer statistics 2020: GLOBOCAN estimates of incidence and mortality worldwide for 36 cancers in 185 countries. CA Cancer J Clin 2021;71(3):209–49.
[2] Llovet JM, et al. Hepatocellular carcinoma. Nat Rev Dis Prim 2021;7(1):6.
[3] Ferrante ND, Pillai A, Singal AG. Update on the diagnosis and treatment of hepatocellular carcinoma. Gastroenterol Hepatol (N Y) 2020;16(10):506–16.
[4] Villanueva A. Hepatocellular carcinoma. New Engl J Med 2019;380(15):1450–62.
[5] McGlynn KA, Petrick JL, London WT. Global epidemiology of hepatocellular carcinoma: an emphasis on demographic and regional variability. Clin Liver Dis 2015;19(2):223–38.
[6] Ma L, et al. Epigenetics in hepatocellular carcinoma: an update and future therapy perspectives. World J Gastroenterol 2014;20(2):333–45.
[7] Cheng AL, et al. Updated efficacy and safety data from IMbrave150: Atezolizumab plus bevacizumab vs. sorafenib for unresectable hepatocellular carcinoma. J Hepatol 2022;76(4):862–73.
[8] Dimri M, Satyanarayana A. Molecular signaling pathways and therapeutic targets in hepatocellular carcinoma. Cancers 2020(2):**12**.
[9] Wei W, et al. Novel celastrol derivatives inhibit the growth of hepatocellular carcinoma patient-derived xenografts. Oncotarget 2014;5(14):5819–31.
[10] Wang L, Zhang Q, You Q. Targeting the HSP90-CDC37-kinase chaperone cycle: a promising therapeutic strategy for cancer. Med Res Rev 2022;42(1):156–82.
[11] Bukau B, Horwich AL. The Hsp70 and Hsp60 chaperone machines. Cell 1998;92(3):351–66.
[12] Hartl FU, Bracher A, Hayer-Hartl M. Molecular chaperones in protein folding and proteostasis. Nature 2011;475(7356):324–32.
[13] Calderwood SK. Cdc37 as a co-chaperone to Hsp90. Subcell Biochem 2015;78:103–12.
[14] Prince TL, et al. Cdc37 as a Co-chaperone to Hsp90. Subcell Biochem 2023;101:141–58.
[15] Nouri-Vaskeh M, et al. The role of HSP90 molecular chaperones in hepatocellular carcinoma. J Cell Physiol 2020;235(12):9110–20.
[16] Serwetnyk MA, Blagg BS. The disruption of protein– protein interactions with co-chaperones and client substrates as a strategy towards Hsp90 inhibition. Acta Pharm Sin B 2021;11(6):1446–68.
[17] Neckers L, Workman P. Hsp90 molecular chaperone inhibitors: are we there yet? Clin Cancer Res 2012;18(1):64–76.
[18] Qvit N, et al. Peptidomimetic therapeutics: scientific approaches and opportunities. Drug Discov Today 2017;22(2):454–62.
[19] Qvit N. Offermanns S, Rosenthal W, editors. *Peptides and Peptidomimetics as Foundations for Drug Discovery*, in *Encyclopedia of Molecular Pharmacology*. Springer; 2021.
[20] Vagner J, Qu H, Hruby VJ. Peptidomimetics, a synthetic tool of drug discovery. Curr Opin Chem Biol 2008;12(3):292–6.
[21] Lenci E, Trabocchi A. Peptidomimetic toolbox for drug discovery. Chem Soc Rev 2020.
[22] Rubin SJ, et al. Conversion of protein active regions into peptidomimetic therapeutic leads using backbone cyclization and cycloscan–how to do it yourself!. Curr Top Med Chem 2018;18(7):556–65.
[23] Rubin SJS, Qvit N. Backbone-cyclized peptides: a critical review. Curr Top Med Chem 2018;18(7):526–55.
[24] Kardani K, et al. Cell penetrating peptides: the potent multi-cargo intracellular carriers. Expert Opin Drug Deliv 2019;16(11):1227–58.
[25] Xie J, et al. Cell-penetrating peptides in diagnosis and treatment of human diseases: from preclinical research to clinical application. Front Pharmacol 2020;11:697.
[26] Bottens RA, Yamada T. Cell-penetrating peptides (CPPs) as therapeutic and diagnostic agents for cancer. Cancers 2022;14(22):5546.
[27] Frankel AD, Pabo CO. Cellular uptake of the tat protein from human immunodeficiency virus. Cell 1988;55(6):1189–93.
[28] Zhou P, et al. HPEPDOCK: a web server for blind peptide-protein docking based on a hierarchical algorithm. Nucleic Acids Res 2018;46(W1):W443–50.
[29] Tao H, et al. Docking cyclic peptides formed by a disulfide bond through a hierarchical strategy. Bioinformatics 2022;38(17):4109–16.
[30] Jumper J, et al. Highly accurate protein structure prediction with AlphaFold. Nature 2021;596(7873):583–9.
[31] Kumar TA. CFSSP: Chou and Fasman secondary structure prediction server. Wide Spectrum 2013;1(9):15–9.
[32] Merrifield RB. Solid phase peptide synthesis I. The synthesis of a tetrapeptide. J Am Chem Soc 1963;85:2149–54.
[33] Gilon C, et al. Backbone cyclization: a new method for conferring conformational constraint on peptides. Biopolym Orig Res Biomol 1991;31(6):745–50.
[34] Aletras A, et al. Preparation of the very acid-sensitive Fmoc-Lys(Mtt)-OH. Application in the synthesis of side-chain to side-chain cyclic peptides and oligolysine cores suitable for the solid-phase assembly of MAPs and TASPs. Int J Pept Protein Res 1995;45(5):488–96.
[35] Lerner Y, et al. Exploring biomolecular interaction between the molecular chaperone hsp90 and its client protein kinase cdc37 using field-effect biosensing technology. JoVE 2022;181:e63495.
[36] Wang L, et al. Optimization and bioevaluation of Cdc37-derived peptides: an insight into Hsp90-Cdc37 protein-protein interaction modulators. Bioorg Med Chem 2017;25(1):233–40.
[37] Cunningham AD, Qvit N, Mochly-Rosen D. Peptides and peptidomimetics as regulators of protein-protein interactions. Curr Opin Struct Biol 2017;44:59–66.
[38] Schrödinger, L. and W. DeLano, *PyMOL, Available at:* ⟨http://www.pymol.org/pymol⟩. 2020.
[39] Peng S, et al. Crystal structure of the middle and C-terminal domains of Hsp90α labeled with a coumarin derivative reveals a potential allosteric binding site as a drug target. Acta Crystallogr D Struct Biol 2022;78(Pt 5):571–85.
[40] Tao H, Zhang Y, Huang SY. Improving protein-peptide docking results via pose-clustering and rescoring with a combined knowledge-based and MM-GBSA scoring function. J Chem Inf Model 2020;60(4):2377–87.
[41] Mochly-Rosen D, Qvit N. Peptide inhibitors of protein-protein interactions. Chim Oggi/Chem Today 2010;28:14–6.
[42] Rubin S, Qvit N. Cyclic peptides for protein-protein interaction targets: applications to human disease. Crit Rev Eukaryot Gene Expr 2016;26(3):199–221.
[43] Frankel, A., et al., TAT-derived transport polypeptide conjugates. 1998.
[44] Bakshi K, et al. Nixon AE, editor. *Circular Dichroism of Peptides*, in *Therapeutic Peptides: Methods and Protocols*. Totowa, NJ: Humana Press; 2014. p. 247–53.
[45] Manning MC, Woody RW. Theoretical CD studies of polypeptide helices: examination of important electronic and geometric factors. Biopolymers 1991;31(5):569–86.
[46] Wang Z, et al. Suppressing the CDC 37 cochaperone in hepatocellular carcinoma cells inhibits cell cycle progression and cell growth. Liver Int 2015;35(4):1403–15.
[47] Augello G, et al. Targeting HSP90 with the small molecule inhibitor AUY922 (luminespib) as a treatment strategy against hepatocellular carcinoma. Int J Cancer 2019;144(10):2613–24.
[48] Nyagol J, et al. The effects of HIV-1 Tat protein on cell cycle during cervical carcinogenesis. Cancer Biol Ther 2006;5(6):684–90.
[49] Huynh D, et al. Oncogenic properties of HIV-Tat in colorectal cancer cells. Curr HIV Res 2007;5(4):403–9.
[50] Conaldi PG, et al. Human immunodeficiency virus-1 tat induces hyperproliferation and dysregulation of renal glomerular epithelial cells. Am J Pathol 2002;161(1):53–61.
[51] Bettaccini AA, et al. Proliferative activity of extracellular HIV-1 Tat protein in human epithelial cells: expression profile of pathogenetically relevant genes. BMC Microbiol 2005;5:20.
[52] Wilkening S, Stahl F, Bader A. Comparison of primary human hepatocytes and hepatoma cell line Hepg2 with regard to their biotransformation properties. Drug Metab Dispos 2003;31(8):1035–42.
[53] Li N, et al. Discovery of novel celastrol-triazole derivatives with Hsp90-Cdc37 disruption to induce tumor cell apoptosis. Bioorg Chem 2021;111:104867.
[54] Huang W, et al. FW-04-806 inhibits proliferation and induces apoptosis in human breast cancer cells by binding to N-terminus of Hsp90 and disrupting Hsp90-Cdc37 complex formation. Mol Cancer 2014;13:150.
[55] Jin L, et al. Discovery of 18β-glycyrrhetinic acid conjugated aminobenzothiazole derivatives as Hsp90-Cdc37 interaction disruptors that inhibit cell migration and reverse drug resistance. Bioorg Med Chem 2018;26(8):1759–75.
[56] Yang S, Liu G. Targeting the Ras/Raf/MEK/ERK pathway in hepatocellular carcinoma. Oncol Lett 2017;13(3):1041–7.
[57] Piatelli MJ, Doughty C, Chiles TC. Requirement for a hsp90 chaperone-dependent MEK1/2-ERK pathway for B cell antigen receptor-induced cyclin D2 expression in mature B lymphocytes. J Biol Chem 2002;277(14):12144–50.